Charge trapping in aligned single-walled carbon nanotube arrays induced by ionizing radiation exposure

Ivan S. Esqueda,[1,a)] Cory D. Cress,[2] Yuchi Che,[3] Yu Cao,[3] and Chongwu Zhou[3]
[1]*Information Sciences Institute, University of Southern California, Arlington, Virginia 22203, USA*
[2]*Electronics Science and Technology Division, Naval Research Laboratory, Washington, DC 20375, USA*
[3]*Department of Electrical Engineering, University of Southern California, Los Angeles, California 90089, USA*

(Received 2 December 2013; accepted 22 January 2014; published online 5 February 2014)

The effects of near-interfacial trapping induced by ionizing radiation exposure of aligned single-walled carbon nanotube (SWCNT) arrays are investigated via measurements of gate hysteresis in the transfer characteristics of aligned SWCNT field-effect transistors. Gate hysteresis is attributed to charge injection (i.e., trapping) from the SWCNTs into radiation-induced traps in regions near the SWCNT/dielectric interface. Self-consistent calculations of surface-potential, carrier density, and trapped charge are used to describe hysteresis as a function of ionizing radiation exposure. Hysteresis width (h) and its dependence on gate sweep range are investigated analytically. The effects of non-uniform trap energy distributions on the relationship between hysteresis, gate sweep range, and total ionizing dose are demonstrated with simulations and verified experimentally. © *2014 AIP Publishing LLC*. [http://dx.doi.org/10.1063/1.4864126]

I. INTRODUCTION

Charge trapping at the interface of single-walled carbon nanotubes (SWCNTs) and dielectric substrates has been attributed as a primary mechanism for instability and non-ideality in the electrostatic and transport properties of CNT-based electronic devices.[1–3] For example, dynamic electric field screening due to charge injection (i.e., trapping) near the SWCNT/dielectric interface is considered a significant contributor to gate hysteresis in the transfer characteristics of SWCNT field-effect transistors (FETs).[4–6] While recent advances in the fabrication and performance of *aligned* SWCNT FET make it a serious candidate for next generation nanoelectronics,[7–9] gate hysteresis remains a significant limitation.[10] The contribution of charge injection to gate hysteresis in SWCNT FETs has been demonstrated experimentally via characterization of the temperature dependence in the transfer characteristics[11] and using atomic force microscopy techniques.[12] Further understanding requires demonstrating the impact of charge injection mechanisms on gate hysteresis as a function of trap buildup and the effect of non-uniform trap energy distributions.

In this paper, we investigate gate hysteresis in the transfer characteristics of aligned SWCNT FETs and the impact of trapping center buildup induced by exposure to ionizing radiation. Measurements of hysteresis as a function of increasing radiation exposure and gate voltage (V_g) sweep range reveal non-uniform buildup in the energy distribution of trapping centers near the SWCNT/dielectric interface. The results are consistent with extensive studies on classical bulk semiconductor/oxide interfaces (e.g., in the Si/SiO_2 system). The analysis and discussion presented in this paper are supported with self-consistent calculations of surface potential and carrier densities in the SWCNTs and generation-recombination statistics at the radiation-induced trapping centers. Calculations of surface potential and carrier densities incorporate the SWCNT band structure, density of states, and quantum capacitance allowing investigating the dependence of charge injection mechanisms on SWCNT diameter and chirality.

II. EXPERIMENTAL RESULTS

Shown in Fig. 1 are the SEM image of the aligned SWCNT arrays and the schematic diagram of the back-gated SWCNT FETs used in this study.[13] The aligned SWCNT FETs were fabricated via a facile transfer method of pre-synthesized nanotubes grown by chemical vapor deposition (CVD). The p-type SWCNT FETs consist of aligned tubes with common back gates, Ti/Pd source and drain contacts and SiO_2 gate dielectrics with a thickness of 50 nm. The SWCNT density is approximately 1 tube/μm with average tube diameter of ~1 nm. We experimentally verified charge injection via near-interfacial donor- and acceptor-like traps through measurements of hysteresis in dual V_g sweeps as a function of the sweep range (V_{gmax}). In these experiments, the forward sweep ranged from $-V_{gmax}$ to V_{gmax} and the reverse sweep from V_{gmax} to $-V_{gmax}$, where $V_{gmax} = 2$, 4, 6, 8, and 10 V. Shown in Fig. 2(a) are the obtained drain current (I_d) vs. gate-to-source voltage (V_{gs}) characteristics for a SWCNT FET with $W = 200\,\mu$m, $L = 2\,\mu$m and using $V_{ds} = -0.1$ V. The inset in Fig. 2(a) plots the relationship between V_{gmax} and the hysteresis width (h) defined as the difference in V_g at $I_d = I_0$ for the reverse and forward V_g sweeps. For the measurements shown here, $I_0 = 100\,\mu$A (e.g., the red arrow in Fig. 2(a) shows the extraction of h for $V_{gmax} = 6$ V). The results in Fig. 2(a) show an increase in h with V_{gmax} attributed larger carrier densities in the SWCNTs contributing to charge injection resulting in accumulation of trapped charges. Additionally, negative voltage shifts in the

a)Author to whom correspondence should be addressed. Electronic mail: isanchez@isi.edu. Tel.: 703-248-6171.

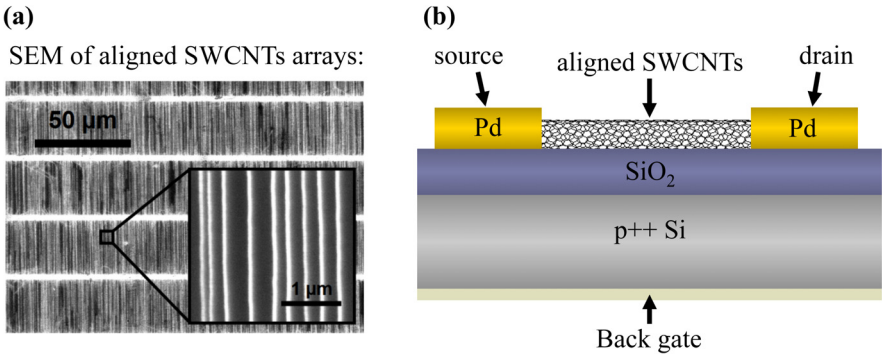

FIG. 1. (a) SEM image of the aligned SWCNT. (b) Schematic diagram of the p-type back-gated SWCNT FETs used in this study. Reprinted with permission from Che *et al.*, "Selective synthesis and device applications of semiconducting single-walled carbon nanotubes using isopropyl alcohol as feedstock," ACS Nano **6**, 7454–7462 (2012). Copyright 2012 American Chemical Society.

forward sweep and positive voltage shifts in the reverse sweep with increasing V_{gmax} are indicative of charge contribution from both donor-like and acceptor-like traps. Donor-like traps are positively charged when ionized (empty) and acceptor-like traps are negatively charged when ionized (occupied).

The SWCNT FETs were irradiated and measured under vacuum eliminating the ambiguities related to ambient moisture and molecular adsorption that may impact hysteresis and cause background SWCNT doping.[14,15] The irradiation vessel was evacuated to a base pressure of $<10^{-5}$ Torr for 24 h (allowing stability in measurements following desorption of residual contaminants in the surface of the CNTs). *In situ* I_d-V_{gs} characterization under vacuum was done at several dose levels up to 2 Mrad(Si) in a ^{60}Co gamma ray source with a dose rate of ~990 rad(Si)/s. Fig. 2(b) plots the I_d-V_{gs} characteristics as a function of total ionizing dose (TID) for a fixed sweep range of $V_{gmax} = 8$ V. In addition to increased h, the results reveal a reduction in transconductance consistent with mobility degradation as a function of TID. At every dose level, the hysteresis width h is extracted from the forward and reverse V_g sweeps for increasing V_{gmax}. Fig. 3(a) plots h as a function of V_{gmax} for increasing levels of TID. The relationship between h and V_{gmax} depends on the energy distribution of the trapping centers since the ionization probability for traps with energy levels closer to the band edges increases with V_{gmax}. In other words, V_{gmax} modulates the energy levels that are accessible for trapping. Therefore, the relationship between h and V_{gmax} for increasing TID provides a way to characterize the energy distribution of the radiation-induced trap buildup. Fig. 3(b) plots the change in h (i.e., $\Delta h = h - h_0$, where h_0 is the hysteresis width prior to irradiation) as a function of TID and for increasing V_{gmax}. These results indicate an increase in h with TID that is more significant for larger V_{gmax}.

III. THEORY

The effects of charge injection on gate hysteresis are described through the generation-recombination of carriers in the nanotube array via the interaction with near-interfacial traps in the gate dielectric with energies distributed within the energy bandgap (E_G) of the semiconducting SWCNTs. Generation-recombination statistics are investigated in context of the electronic properties of the SWCNTs. This section begins with describing calculations of bandstructure and DOS for SWCNTs then continues with calculations for capacitance and electrostatic potential for an array of aligned SWCNTs. Finally, charge trapping mechanisms are incorporated into the presented formulation, which is then used to demonstrate static and transient effects of traps near the SWCNT/dielectric interface.

A. SWCNT band structure and density of states

The bandstructure is obtained from the nearest-neighbor tight-binding (NNTB) E-k formalism because of simplicity in the analytical calculations and demonstrated accuracy to

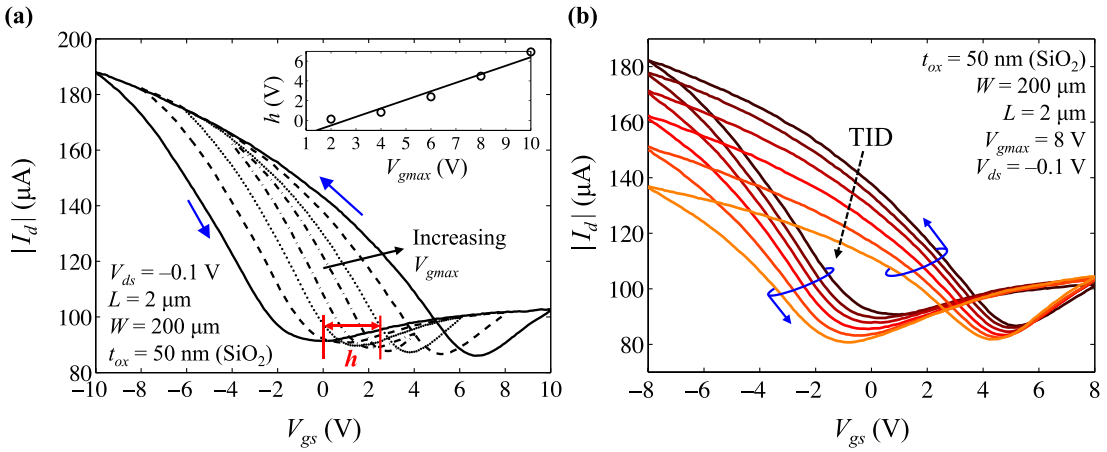

FIG. 2. (a) Drain current (I_d) vs. gate-to-source voltage (V_{gs}) characteristics for a SWCNT FET with $W = 200\,\mu$m, $L = 2\,\mu$m and using $V_{ds} = -0.1$ V and increasing the gate-voltage sweep range (V_{gmax}). The inset plots the relationship between V_{gmax} and the hysteresis width (h). (b) I_d-V_{gs} characteristics as a function of TID for fixed V_{gmax}.

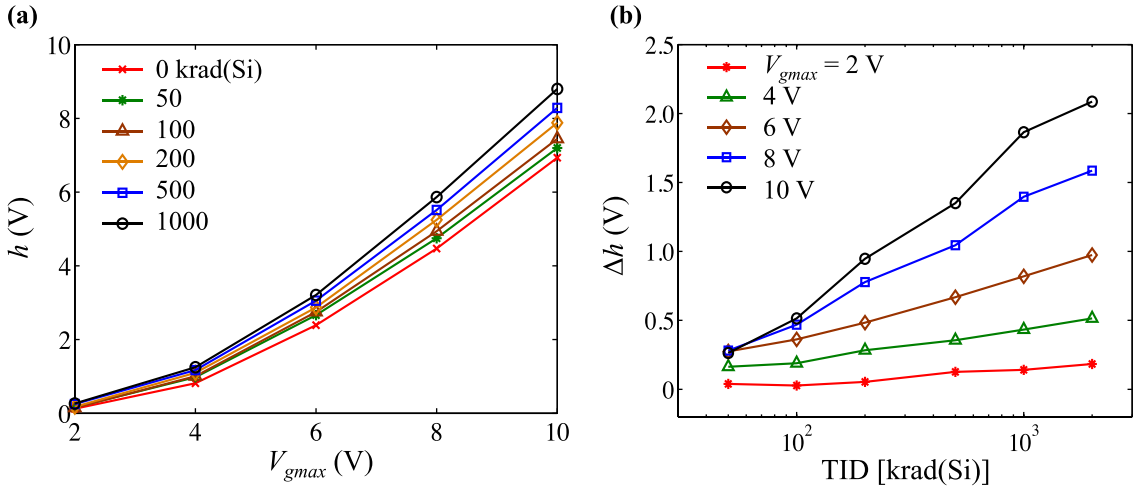

FIG. 3. (a) Hysteresis width (h) plotted as a function of V_{gmax} for increasing levels of TID. (b) Change in h (i.e., $\Delta h = h - h_0$) as a function of TID and for increasing V_{gmax}.

reproduce first-principle calculations for low-energy conditions in SWCNTs with diameters ≥1 nm. The NNTB energy dispersion is given by

$$E(\mathbf{k}) = \pm\gamma\sqrt{1 + 4\cos\left(\frac{\sqrt{3}a}{2}k_x\right)\cos\left(\frac{a}{2}k_y\right) + 4\cos^2\left(\frac{a}{2}k_y\right)}, \tag{1}$$

where k_x and k_y are the CNT Brillouin zone wavevector x and y components and $a = \sqrt{3}a_{C-C}$, where $a_{C-C} = 1.42$ Å is the carbon-carbon bond length.[16,17] The allowed wavevectors are constructed from the reciprocal lattice vectors along the SWCNT axial ($\mathbf{K}_a$) and circumferential ($\mathbf{K}_c$) directions as $\mathbf{k} = (kT_r/2\pi)\mathbf{K}_a + j\mathbf{K}_c$.[18] Here, k and j represent the allowed wavevectors within the CNT Brillouin zone. Restrictions on the wavevectors that result from boundary conditions on the Bloch wave functions result in N one-dimensional (1-D) sub-bands that are quantized along the circumferential direction of the SWCNT but continuous along the axial direction as $k = (-\pi/T_r,\ \pi/T_r)$, where T_r is the magnitude of the SWCNT translation vector.[19]

The density of states $g(E)$ for SWCNTs is determined numerically from the sum of the contributions from each of the energy sub-bands as

$$g(E) = \sum_{j=1}^{N} g(E,j) = \sum_{j=1}^{N} \frac{1}{\pi}\left|\frac{\partial k}{\partial E}\right|. \tag{2}$$

The density of states calculation for the SWCNT results in a divergence of $g(E, j)$ when the gradient of E vanishes. This gives several singularities in the $g(E)$ relationship known as van-Hove singularities (VHS) due to the contributions from the different energy sub-bands that are characteristic of 1-D materials. Fig. 4 shows the bandstructure and density of states calculations for a (13, 0) CNT. Fig. 4(a) plots the 1st three (double degenerate) energy sub-bands as a function of the wavevector and Fig. 4(b) plots $g(E)$ showing VHS at the lowest energy from each one of the sub-bands.

B. SWCNT capacitance and surface potential in aligned SWCNT arrays

Analyzing the electronic properties in arrays of aligned SWCNTs requires calculating the electrostatic channel potential (or surface potential, i.e., ψ_s) of individual SWCNT. This is a function of the capacitance per unit length (C_{CNT}) of a single tube in the array and depends on device geometry. C_{CNT} consists of the series combination of two components, the quantum capacitance (C_q) and the electrostatic capacitance (C_{es}) and is, therefore, given by $C_{CNT}^{-1} = C_q^{-1} + C_{es}^{-1}$.[20] The quantum capacitance is given by the change in charge density with surface potential and can be obtained numerically as

$$C_q = \frac{q^2}{4k_BT}\int_{-\infty}^{\infty} g(E)\,\mathrm{sech}^2\left(\frac{E - q\psi_s}{2k_BT}\right)dE. \tag{3}$$

Here, q is the electronic charge, k_B is the Boltzmann constant, and T is temperature.[18,21] The electrostatic capacitance has been recently derived for a SWCNT from an infinite array of aligned tubes with uniform spacing ($1/d$) and is given by

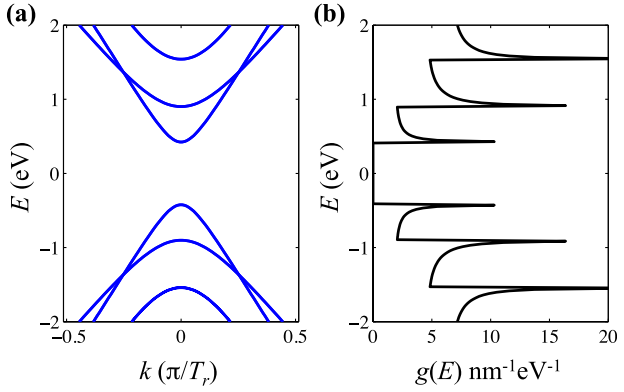

FIG. 4. (a) Band structure for a (13,0) zigzag SWCNT showing the 1st three (doubly degenerate) 1-D energy sub-bands. (b) Density of states calculation from the sum of the contributions of the 1st three sub-bands.

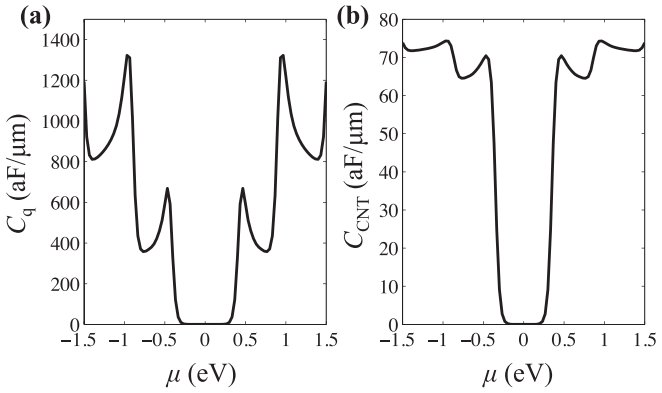

FIG. 5. Calculation of quantum capacitance (a) and CNT capacitance (b) for a (13,0) SWCNT plotted as a function of the normalized chemical potential (i.e., μ/kT). C_{CNT} calculations are for a single tube from an array of aligned SWCNTs with density $d = 1\,\mu m^{-1}$ on a dielectric with thickness $t_d = 8$ nm and dielectric constant $K_d = 3.9$ (i.e., SiO_2).

$$C_{es} = \frac{2\pi\varepsilon_0 K_d}{\log\left[\frac{\sinh(2\pi t_d d)}{\pi r d}\right]}, \tag{4}$$

where ε_0 is the vacuum permittivity, K_d is the dielectric constant, t_d is the thickness of the dielectric layer, d is the density, and r is the radius of the SWCNTs.[20] Fig. 5 plots C_q and C_{CNT} as a function of the chemical potential $\mu = q\psi_s$ for a (13, 0) SWCNT. These calculations are for $t_d = 8$ nm, $K_d = 3.9$, and $d = 1\,\mu m^{-1}$ (i.e., $C_{es} \approx 78$ aF/μm).

Surface potential is determined from the capacitive coupling of the gate voltage (V_g) to the SWCNT as given by

$$\psi_s = (V_g - V_{fb})\left(\frac{C_{es}}{C_{es} + C_q}\right) = V_g - V_{fb} - V_{ox}. \tag{5}$$

Here, V_{fb} is the flatband and V_{ox} is the voltage drop in the dielectric. The energy band diagram of the gate-dielectric-SWCNT system shown in Fig. 6 provides a schematic depiction of the relationship between ψ_s, V_g, V_{fb}, and V_{ox}. In Fig. 6, only the bottom of the conduction band (E_{Cb}) and top of the valence band (E_{Vt}) from the 1st sub-band are shown.

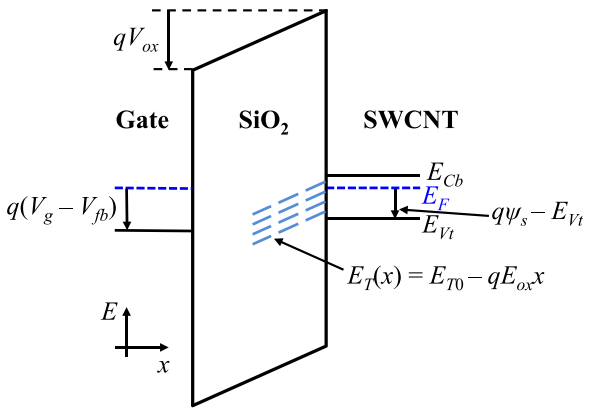

FIG. 6. Energy band diagram for the gate-dielectric-SWCNT system. In this diagram, $(V_g - V_{fb})$ is positive, therefore V_{ox} and ψ_s are also positive. In the presence of an oxide electric field (E_{ox}), the trap energy level E_T varies with distance from the SWCNT/SiO_2 interface.

The $\psi_s(V_g)$ relationship in Eq. (5) is implicit in ψ_s and must be solved numerically. Shown in Fig. 7 are calculations of ψ_s and V_{ox} for a (13, 0) SWCNT from an array with $d = 1\,\mu m^{-1}$, $t_d = 8$ nm, and $K_d = 3.9$. At low gate voltages $C_q \ll C_{es}$ and ψ_s is approximately linear with $(V_g - V_{fb})$. For higher $\pm V_g$ the charge in the SWCNT and C_q increases rapidly pinning ψ_s. At these higher values of $\pm V_g$ (e.g., $\sim \pm 1$ V in Fig. 4), most of the voltage drop is across the oxide.

C. Trapping at the SWCNT/dielectric interface

This section describes how charge-trapping mechanisms are incorporated into the calculations of SWCNT electrostatic potential (i.e., ψ_s). V_{fb} accounts for the difference in workfunction between the gate and the SWCNT (i.e., Φ_{MC}) and is equal to the gate voltage required for ψ_s to be zero. When charge is trapped in the dielectric layer, there is an additional shift in the SWCNT flatband voltage proportional to the effective number of charges trapped per unit length (i.e., N_t). The flatband voltage is expressed as

$$V_{fb} = \Phi_{MC} - \frac{qN_t}{C_{es}}, \tag{6}$$

where N_t is a combination of net effective ionized donor-like traps (N_{td}) and net effective ionized acceptor-like traps (N_{ta}). N_{td} and N_{ta} are obtained by integrating the position and energy distribution of ionized donor-like and acceptor-like traps as given by

$$N_t = N_{td} - N_{ta} = \int_0^{t_d}\int_{-\infty}^{\infty} \frac{x}{t_d} p_{td}(x,E)dE\,dx - \int_0^{t_d}\int_{-\infty}^{\infty} \frac{x}{t_d} n_{ta}(x,E)dE\,dx. \tag{7}$$

Here, p_{td} and n_{ta} are the areal densities of ionized donor-like and acceptor-like traps (units are $cm^{-2}eV^{-1}$) and have different sign since ionized donor-like traps are positively charged and ionized acceptor-like traps are negatively charged. Applying Gauss's law accounts for charges near the SWCNT/dielectric interface having a greater effect on V_{fb} than charges away from the interface. In this x-axis,

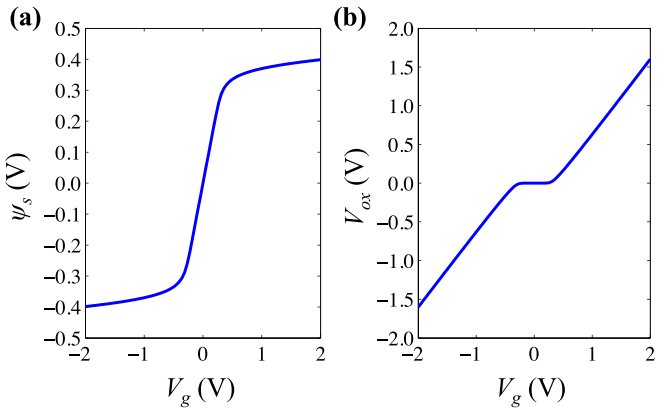

FIG. 7. (a) Surface potential (ψ_s) calculations as a function of gate voltage for a (13,0) zigzag SWCNT from an array with density of $1\,\mu m^{-1}$ and an 8 nm thick SiO_2 gate dielectric. (b) Voltage drop in the oxide (V_{ox}) as a function of gate voltage.

definition $x=0$ at the gate/dielectric interface and $x=t_d$ at the CNT/dielectric interface. The formulation of N_t approximates the back-gate/dielectric/SWCNT single tube system as a planar structure with gate width equivalent to the arc length of a cylindrical nanotube device (i.e., $W \approx \theta t_d$, where θ is the CNT azimuthal angle over which the device is approximated by a planar structure).

Transient charge trapping mechanisms are described in terms of recombination-generation statistics at the SWCNT/dielectric interface. The ionization rates for acceptor-like and donor-like traps are given by the time rate of change in the SWCNT electron and hole concentrations due to generation and recombination mechanisms and are expressed as[22]

$$\frac{dp_{td}}{dt} = c_p\left[n_{td}p - p_{td}pe^{(E_F-E_{Td})/kT}\right] - c_n\left[p_{td}n - n_{td}ne^{(E_{Td}-E_F)/kT}\right], \tag{8a}$$

$$\frac{dn_{ta}}{dt} = c_n\left[p_{ta}n - n_{ta}ne^{(E_{Ta}-E_F)/kT}\right] - c_p\left[n_{ta}p - p_{ta}pe^{(E_F-E_{Ta})/kT}\right]. \tag{8b}$$

In this notation, n and p are the SWCNT electron and hole carrier concentration per unit length, n_t and p_t are the number of occupied and empty traps per gate dielectric unit area per eV, c_n and c_p are the electron and hole capture coefficients, and E_T is the trap energy level referenced to E_F. The total number of available traps is given by the sum of occupied and empty traps, i.e., $D_T = n_t + p_t$. The subscripts d and a denote donor and acceptor traps. The electron and hole concentrations are, respectively, calculated as the total number of occupied energy states in the conduction and the total number of empty energy states in the valence band and are given by[23]

$$n = \int_{-\infty}^{\infty} F(E,\psi_s)g(E)dE, \tag{9a}$$

$$p = \int_{-\infty}^{\infty} [1-F(E,\psi_s)]g(E)dE, \tag{9b}$$

where $F(E, \psi_s)$ is the Fermi-Dirac distribution function given by

$$F(E,\psi_s) = \frac{1}{1+e^{(E-q\psi_s)/k_BT}}. \tag{10}$$

From units considerations, electron and hole capture coefficients must have dimensions of 1/(concentration-time) or cm/s. Additionally, for traps located within the dielectric layer, the capture coefficients are reduced by a factor that increases exponentially with distance from the SWCNT/dielectric interface. This factor comes from the WKB approximation for quantum-mechanical tunneling from the SWCNT to the trap across the classically forbidden dielectric region. The electron and hole capture coefficients are expressed as

$$c_n = c_{n0}e^{-2\kappa_0 x}, \tag{11a}$$

$$c_p = c_{p0}e^{-2\kappa_0 x}, \tag{11b}$$

where c_{n0} and c_{p0} are constants and κ_0 is a function of the potential barrier at the CNT/dielectric interface (ϕ_B) and is given by $\kappa_0^2 = 2m^*\phi_B/\hbar^2$. For SiO_2, $1/\kappa_0 \approx 1.7$ Å.[22]

IV. CALCULATIONS AND DISCUSSION

Fig. 8 plots ψ_s, C_{CNT}, and the density of trapped charges (N_{td}, N_{ta}) as a function of V_g for increasing densities of donor-like and acceptor-like traps (i.e., $D_T = D_{TA} = D_{TD}$). These results are from self-consistent calculations of ψ_s and trap generation-recombination statistics under *steady state conditions* (i.e., $dp_{td}/dt = dn_{ta}/dt = 0$). The calculations in Fig. 8 are for a (13,0) zigzag SWCNT with uniformly distributed traps (in position and energy) and a dielectric layer with thickness of $t_d = 8$ nm. Traps in the upper half of the bandgap are acceptor-like and traps in the lower half of the bandgap are donor-like (i.e., traps are amphoteric). The results in Fig. 8 demonstrate the effects of trapping as a function of the

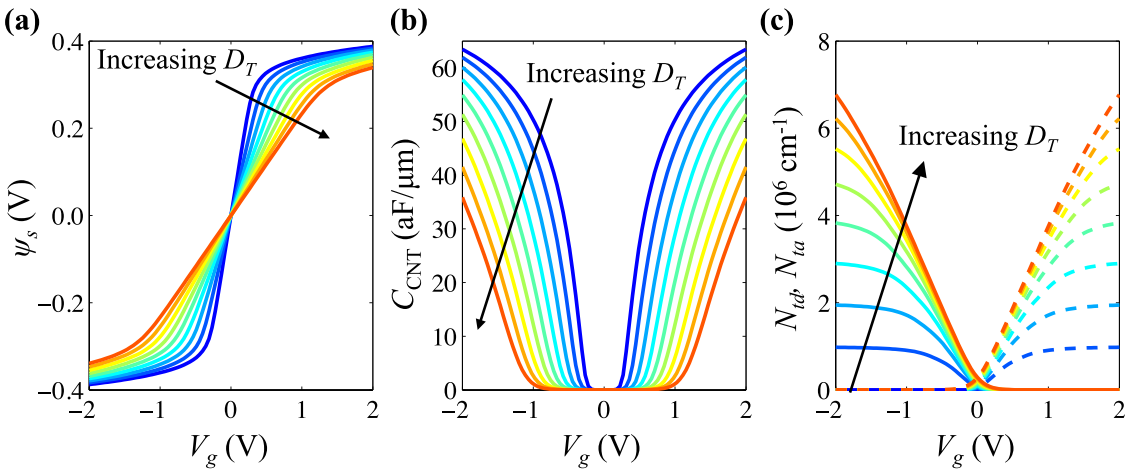

FIG. 8. Steady state calculations of (a) surface potential, (b) SWCNT capacitance, and (c) density of trapped charges plotted (solid lines are donors and dashed lines are acceptors) as a function of gate voltage for increasing trap density D_T. Traps are uniformly distributed in position and energy within ±0.5 eV with acceptor-like traps in the upper half and donor-like traps in the lower half. Calculations are for a (13,0) zigzag SWCNT in an array with density of 1 nanotube/μm and $t_d = 8$ nm.

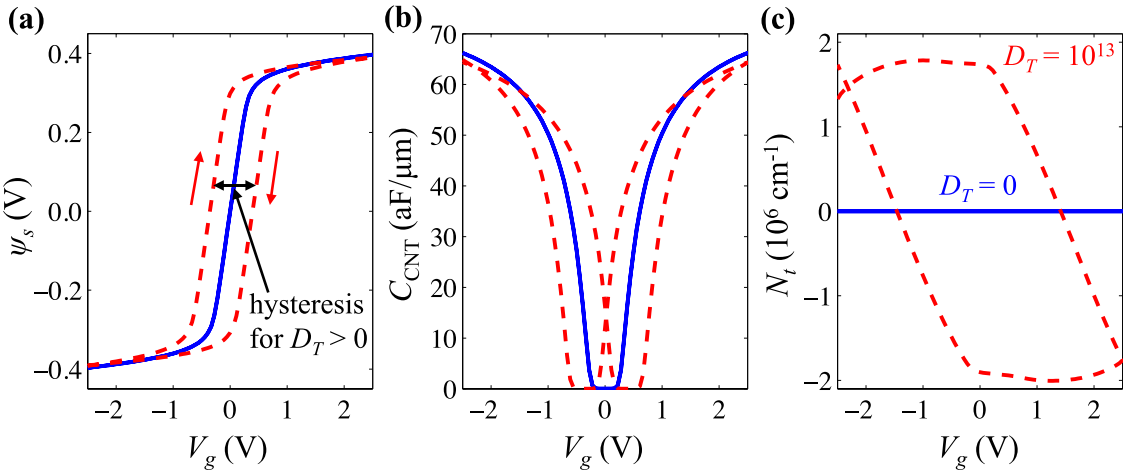

FIG. 9. Transient calculations of (a) ψ_s, (b) C_{CNT}, and (c) $N_t = N_{td} - N_{ta}$ plotted as a function of gate voltage for no traps (i.e., $D_T = 0$) and for a uniform distribution of traps within ±0.5 eV (acceptor-like traps in the upper half and donor-like traps in the lower half). Calculations are for a (13,0) zigzag SWCNT in an array with density of 1 nanotube/μm and $t_d = 8$ nm.

gate bias resulting from the modulation of ψ_s changing the trap occupancy. Negative V_g values raise the hole concentration and the density of ionized donor-like traps (solid lines in Fig. 8(c)) that contribute positive charge. The increased net positive charge contribution due to N_{td} results in negative shifts in the electrical characteristics as shown in Figs. 8(a) and 8(b). On the other hand, positive V_g values result in a greater density of negatively charged ionized acceptor-like traps (dashed lines in Fig. 8(c)) with the opposite effect on the electrical characteristics (i.e., positive shifts). Traps with small capture/emission times (i.e., recombination-generation mechanism will reach steady state for a given measurement condition) will not result in gate hysteresis but will cause shifts and vary the slope of the electrical characteristics as a function of trap density as shown in Fig. 8.

The transient effects of recombination-generation statistics are investigated through self-consistent calculations of surface potential, capacitance, and trapping mechanisms as described by the trap ionization rates. A voltage sweep rate is specified (V_{sw} in units of V/s), from which the time per voltage step is obtained (t_{step}). For N number of voltage steps $t_{step} = (V_{gmax} - V_{gmin})/(NV_{sw})$. For each voltage step, self-consistent calculations are performed based on finite difference time discretization using an implicit time-stepping scheme.[24] Dual V_g sweeps are simulated to investigate hysteresis effects on the SWCNT electrical characteristics. Shown in Fig. 9 are transient calculations of ψ_s, C_{CNT}, and $N_t = N_{td} - N_{ta}$ as a function of V_g for no traps (i.e., $D_T = 0\,\text{cm}^{-2}\,\text{eV}^{-1}$) and for a uniform distribution of traps within ±0.5 eV. The results in Fig. 9 are for a voltage sweep rate of $V_{sw} = 0.33$ V/s and reveal the effects of gate hysteresis. As before, the calculations in Fig. 9 are for a (13,0) zigzag SWCNT with uniformly distributed amphoteric traps and $t_d = 8$ nm. The values for c_{n0} and c_{p0} give capture times on the order of milliseconds to seconds for reasonable values of carrier concentrations (i.e., when device is "on") consistent with experimental observations.[3]

The effects of trap non-uniform energy distribution on the relationship between hysteresis width (h) and V_{gmax} are investigated analytically through simulations of transient trapping mechanisms. Fig. 10 shows calculations of h as a function of V_{gmax} for different energy distributions of near-interfacial traps. Fig. 10(a) plots the trap energy distributions (i.e., uniform, linear, quadratic, and exponential distributions) where all distributions are normalized to the same total number of traps per unit area (i.e., the integral of $D_T(E_T)$ is fixed) and Fig. 10(b) plots the calculations of h as a function of V_{gmax} for the different distributions and for increasing values of the normalized D_T. In these calculations, h has been extracted as

$$h = \left[\left. \frac{qN_t}{C_{es}} \right|_{V_g(\psi_s=0)\uparrow} - \left. \frac{qN_t}{C_{es}} \right|_{V_g(\psi_s=0)\downarrow} \right], \tag{12}$$

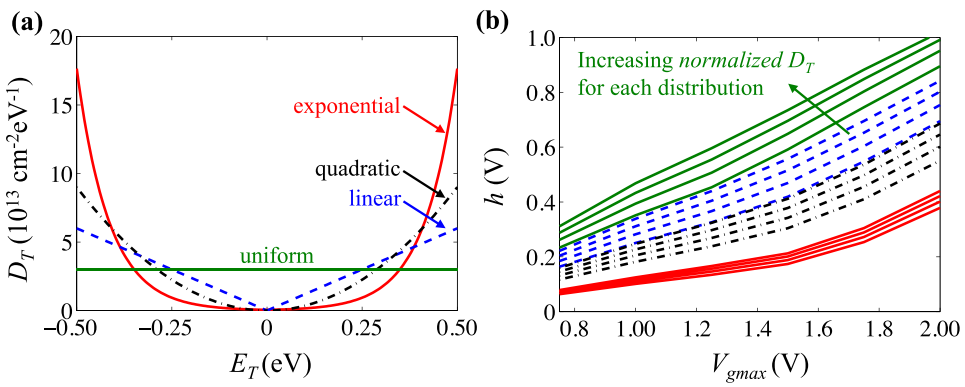

FIG. 10. Simulations of hysteresis width (h) as a function of V_{gmax} for different energy distributions of near-interfacial traps (acceptor-like traps in the upper half and donor-like traps in the lower half). Calculations are for a (13,0) zigzag SWCNT in an array with density of 1 nanotube/μm and $t_d = 8$ nm.

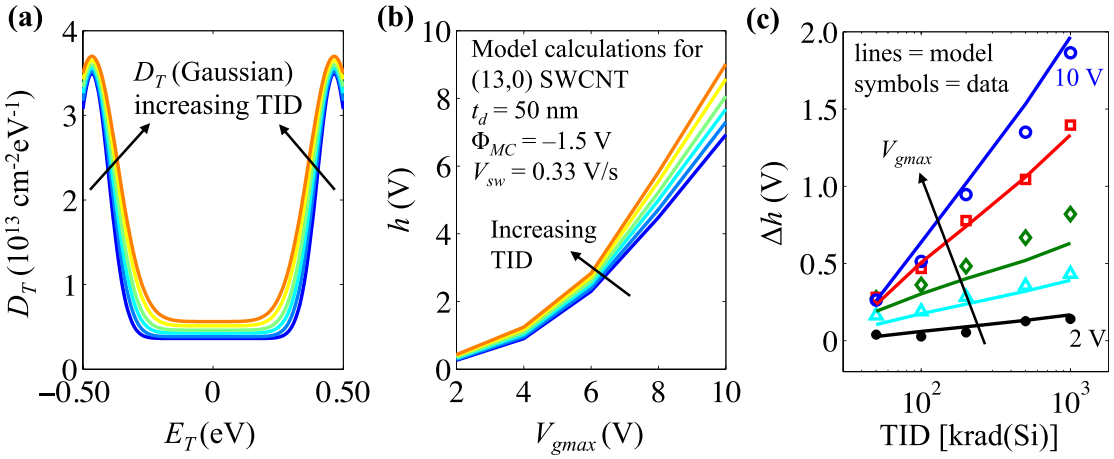

FIG. 11. (a) Simulated non-uniform D_T distributions increasing with TID. (b) Model calculations of hysteresis width as a function of V_{gmax} for increasing TID. (c) Comparison of simulated and measured increase in hysteresis width (h) as a function of TID and V_{gmax}. Model calculations are for a (13,0) zigzag SWCNT in an array with density of 1 nanotube/μm and $t_d = 50$ nm.

which is equivalent to the difference in V_g intercept at $\psi_s = 0$ for the simulated positive and negative gate sweeps and accounts for voltage shifts due to ionized donor-like and acceptor like traps. For the case of uniform D_T, the trap density is increased equally for all energies and the charge contribution from ionized traps results in similar increments in h for all values of V_{gmax}. On the other hand, the increase in h as a function of trap density has a stronger dependence on V_{gmax} for non-uniform D_T energy distributions (i.e., for linear, quadratic, and exponential distributions). This is due to a greater buildup in trap density specified near the band edges where they are more likely to be ionized with increasing V_{gmax}. In fact, good qualitative agreement between simulations and experimental data can be obtained using a "U-shaped" non-uniform energy distribution of D_T within 15 nm from the SWCNT/SiO_2 interface ($t_d = 50$ nm in the measured SWCNT FETs). In this comparison, we assume that mostly the semiconducting tubes contribute to hysteresis and we use a (13, 0) SWCNT from an array of aligned tubes with density $d = 1\ \mu m^{-1}$ to describe their average hysteresis contribution. The U-shaped energy distribution of D_T is modeled with Gaussian components near the band edges. Shown in Fig. 11(a) is the simulated non-uniform distribution of interface traps and the buildup as a function of total ionizing dose. Calculations of hysteresis width as a function of V_{gmax} for the simulated D_T are shown in Fig. 11(b). Finally, the comparison with experimental data is given for the increase in hysteresis width (Δh) as a function of TID for various values of V_{gmax} with good qualitative agreement. Near-interfacial traps with similar U-shaped energy distributions have been used in other semiconductor/oxide systems resulting in good agreements with experimental data.[25–27]

V. CONCLUSIONS

The effects of near-interfacial trapping induced by ionizing radiation exposure of aligned SWCNT arrays are investigated via measurements of gate hysteresis in the transfer characteristics of aligned SWCNT FETs. Gate hysteresis is attributed to charge injection from the SWCNTs into radiation-induced traps in regions near the SWCNT/dielectric interface. Measurements reveal an increase in hysteresis width (h) with gate voltage sweep range (V_{gmax}) attributed to larger carrier densities in the SWCNTs contributing to charge injection resulting in accumulation of trapped charges. Additionally, the relationship between h and V_{gmax} depends on the energy distribution of the trapping centers since the ionization probability for traps with energy levels closer to the band edges increases with V_{gmax}. In other words, V_{gmax} modulates the energy levels that are accessible for trapping. Thus, the effects on non-uniform trap buildup are characterized via the dependence of h on V_{gmax} as a function of ionizing radiation exposure. Exposed SWCNT FETs reveal a more pronounced increase in hysteresis as a function of TID for measurements with larger V_{gmax}. Reduced transconductance ($g_m \sim \partial I_d/\partial V_g$) and negative voltage shifts in the I_d-V_{gs} characteristics are also measured as a function of TID. These results are, respectively, attributed to degraded carrier mobility (e.g., due to increased Coulomb scattering from trapped charge) and to radiation-induced fixed charge (i.e., hole trapping) in the bulk of the gate oxide.

The effects of charge injection on gate hysteresis are described through the generation-recombination of carriers in the nanotube array via the interaction with near-interfacial traps in the gate dielectric with energies distributed within the energy bandgap (E_G) of the semiconducting SWCNTs. Self-consistent calculations of surface-potential, carrier density, and trapped charge are used to describe hysteresis as a function of ionizing radiation exposure. The calculations demonstrate the relationship between hysteresis width and trap density (D_T) resulting in a stronger dependence on V_{gmax} for non-uniform D_T energy distributions. Good agreement between theory and experimental data is obtained with a "U-shaped" non-uniform energy distribution of D_T described through Gaussian components near the band edges located within 15 nm from the SWCNT/SiO_2 interface.

ACKNOWLEDGMENTS

This work was supported (in part) by the Defense Threat Reduction Agency, Basic Research Award No.

HDTRA1-10-1-0015, to the USC Information Sciences Institute and the University of Southern California.

[1]W. Kim, A. Javey, O. Vermesh, Q. Wang, Y. Li, and H. Dai, "Hysteresis caused by water molecules in carbon nanotube field-effect transistors," Nano Lett. **3**(2), 193–198 (2003).
[2]K. Bradley, J. Cumings, A. Star, J.-C. P. Gabriel, and G. Grüner, "Influence of mobile ions on nanotube based FET devices," Nano Lett. **3**(5), 639–641 (2003).
[3]A. Robert-Peillard and S. V. Rotkin, "Modeling hysteresis phenomena in nanotube field-effect transistors," IEEE Trans. Nanotechnol. **4**(2), 284–288 (2005).
[4]S. Kar, A. Vijayaraghavan, C. Soldano, S. Talapatra, R. Vajtai, O. Nalamasu, and P. M. Ajayan, "Quantitative analysis of hysteresis in carbon nanotube field-effect devices," J. Appl. Phys. **89**, 132118 (2006).
[5]H. Hongo, F. Nihey, and S. Yorozu, "Relationship between carbon nanotube density and hysteresis characteristics of carbon nanotube random network-channel field effect transistors," J. Appl. Phys. **107**(9), 094501 (2010).
[6]D. Estrada, S. Dutta, A. Liao, and E. Pop, "Reduction of hysteresis for carbon nanotube mobility measurements using pulsed characterization," Nanotechnology **21**, 085702 (2010).
[7]C. Wang, K. Ryu, L. G. Arco, A. Badmaev, J. Zhang, X. Lin, Y. Che, and C. Zhou, "Synthesis and device applications of high-density aligned carbon nanotubes using low-pressure chemical vapor deposition and stacked multiple transfer," Nano Res. **3**, 831–842 (2010).
[8]K. Ryu, A. Badmaev, C. Wang, A. Lin, N. Patil, L. Gomez, A. Kumar, S. Mitra, H.-S. P. Wong, and C. Zhou, "CMOS-analogous wafer-scale nanotube-on-insulator approach for submicrometer devices and integrated circuits using aligned nanotubes," Nano Lett. **9**(1), 189–197 (2009).
[9]Y. Che, A. Badmaev, A. Jooyaie, T. Wu, J. Zhang, C. Wang, K. Galatsis, H. A. Enaya, and C. Zhou, "Self-aligned T-gate high-purity semiconducting carbon nanotube RF transistors operated in quasi-ballistic transport and quantum capacitance regime," ACS Nano **6**, 6936–6943 (2012).
[10]I. S. Esqueda, Y. Fu, C. D. Cress, J. Zhang, C. Zhou, J. Ahlbin, M. Bajura, G. Boverman, and M. Fritze, "Modeling the effects of hysteresis on aligned nanotube FETs exposed to ionizing radiation," in Proceedings of the Radiation Effects on Components and Systems (RADECS) Conference, September 2012.
[11]A. Vijayaraghavan, S. Kar, C. Soldano, S. Talapatra, O. Nalamasu, and P. M. Ajayan, "Charge-injection-induced dynamic screening and origin of hysteresis in field-modulated transport in single-wall carbon nanotubes," Appl. Phys. Lett. **89**, 162108-3 (2006).
[12]J. J. McMorrow, C. D. Cress, and C. A. Affouda, "Charge injection in high-k gate dielectrics of single-walled carbon nanotube thin-film transistors," ACS Nano **6**(6), 5040–5050 (2012).
[13]Y. Che, C. Wang, J. Liu, B. Liu, X. Lin, J. Parker, C. Beasley, H. S. P. Wong, and C. Zhou, "Selective synthesis and device applications of semiconducting single-walled carbon nanotubes using isopropyl alcohol as feedstock," ACS Nano **6**, 7454–7462 (2012).
[14]J. S. Lee, S. Ryu, K. Yoo, I. S. Choi, W. S. Yun, and J. Kim, "Origin of gate hysteresis in carbon nanotube field-effect transistors," J. Phys. Chem. C **111**, 12504–12507 (2007).
[15]H. Lin and S. Tiwari, "Localized charge trapping due to adsorption in nanotube field-effect transistor and its field-mediated transport," Appl. Phys. Lett. **89**, 073507-3 (2006).
[16]R. Saito, G. Dresselhaus, and M. S. Dresselhaus, *Physical Properties of Carbon Nanotubes* (Imperial, London, 1998).
[17]P. R. Wallace, "The band theory of graphite," Phys. Rev. **71**, 622–634 (1947).
[18]H.-S. P. Wong and D. Akinwande, *Carbon Nanotube and Graphene Device Physics* (Cambridge University Press, 2011).
[19]A. Rochefort, D. R. Salahub, and P. Avouris, "Effects of finite length on the electronic structure of carbon nanotubes," J. Phys. Chem. B **103**, 641–646 (1999).
[20]S. J. Kang, C. Kocabas, T. Ozel, M. Shim, N. Pimparkar, M. A. Alam, S. V. Rotkin, and J. A. Rogers, "High-performance electronics using dense, perfectly aligned arrays of single-walled carbon nanotubes," Nat. Nanotechnol. **2**, 230–236 (2007).
[21]D. Akinwande, Y. Nishi, and H.-S. P. Wong, "Analytical model of carbon nanotube electrostatics: Density of states, effective mass, carrier density and quantum capacitance," in *IEEE IEDM Technical Digest* (2007), p. 753.
[22]F. Heiman and G. Warfield, "The effects of oxide traps on the MOS capacitance," IEEE Trans. Electron Devices **12**(4), 167–178 (1965).
[23]R. F. Pierret, *Advanced Semiconductor Fundamentals*, 2nd ed. (Prentice-Hall, 2003).
[24]C. M. Snowden, *Introduction to Semiconductor Device Modeling* (World Scientific, 1986).
[25]I. S. Esqueda and H. J. Barnaby, "Modeling the non-uniform distribution of radiation-induced interface traps," IEEE Trans. Nucl. Sci. **59**(4), 723–727 (2012).
[26]R. da Silva, G. I. Wirth, and L. Brusamarello, "An appropriate model for the noise power spectrum produced by traps at the Si-SiO2 interface: A study of the influence of a time-dependent Fermi level," J. Stat. Mech. **2008**, P10015.
[27]V. Djara, T. P. O'Regan, K. Cherkaoui, M. Schmidt, S. Monaghan, É. O'Connor, I. M. Povey, D. O'Connell, M. E. Pemble, and P. K. Hurley, "Electrically active interface defects in the $In_{0.53}Ga_{0.47}As$ MOS system," Microelectron. Eng. **109**, 182–188 (2013).